Quasinormal modes of Schwarzschild black holes on the real axis

Koutarou Kyutoku,[1,2,3] Hayato Motohashi,[4] and Takahiro Tanaka[1,2]

[1]*Department of Physics, Kyoto University, Kyoto 606-8502, Japan*

[2]*Center for Gravitational Physics and Quantum Information, Yukawa Institute for Theoretical Physics, Kyoto University, Kyoto 606-8502, Japan*

[3]*Interdisciplinary Theoretical and Mathematical Sciences Program (iTHEMS), RIKEN, Wako, Saitama 351-0198, Japan*

[4]*Division of Liberal Arts, Kogakuin University, 2665-1 Nakano-machi, Hachioji, Tokyo 192-0015, Japan*

(Received 13 June 2022; accepted 23 January 2023; published 7 February 2023)

We study the scattering of gravitational waves by a Schwarzschild black hole and its perturbed siblings to investigate influences of proposed spectral instability of quasinormal modes on the ringdown signal. Our results indicate that information of dominant ringdown signals, which are ascribed to the fundamental (i.e., least damping) quasinormal mode of unperturbed Schwarzschild black holes, is imprinted in the phase shift defined from the transmission amplitude ($1/A_{\rm in}$ in our notation). This approximately parallels the fact that the resonance of quantum systems is imprinted in the phase shift of the S matrix. The phase shift around the oscillation frequency of the fundamental mode is modified only perturbatively even if the quasinormal-mode spectrum is destabilized by a perturbative bump at a distant location, signifying the stability of the ringdown signal. At the same time, the phase shift at low frequencies is modulated substantially reflecting the late-time excitation of echo signals associated with the quasinormal-mode spectrum after destabilization.

DOI: 10.1103/PhysRevD.107.044012

I. INTRODUCTION

Quasinormal modes are believed to play a central role in clarifying various properties of black hole spacetimes (see, e.g., Refs. [1,2] for reviews). Physically, quasinormal modes are exponentially decaying monochromatic waves escaping to null infinity and to the event horizon. They are excited in a universal manner as a response to impinging fields [3–5] and/or the motion of matter [6–9], and associated observable signals are called the ringdown signals. Individual modes are characterized by a complex frequency, i.e., the oscillation frequency and the decay width (or damping time). Because they are determined by the mass and the spin for Kerr (including Schwarzschild) black holes, analysis of the ringdown signals tells us these two parameters [10,11]. Remarkably, because the mass and the spin completely determine all the quasinormal modes, consistency assessment of estimated parameters for individual modes will enable us to test whether astrophysical black holes are really represented by Kerr black holes in general relativity [12,13]. Furthermore, quasinormal-mode spectra are expected to provide us with a hint to quantum gravity [14–16].

In the last few years, it has been argued that the quasinormal-mode spectrum could be destabilized by tiny perturbations to the potential of various types [17–19]. In particular, even the fundamental mode is destabilized when the potential is modified at a large distance from the black hole [18], dating back to Ref. [20] (see also Refs. [21,22]). In realistic situations, excitation of quasinormal modes is inevitably accompanied by nontrivial perturbations due to the dynamical formation process of a deformed black hole and/or surrounding material. Thus, the spectral instability of quasinormal modes could be fatal to the program of black hole spectroscopy.

However, the spectral instability of quasinormal-mode spectra does not destabilize observable ringdown signals, particularly on the damping time scale of unperturbed quasinormal modes [23,24]. Rather, a lot of evidence is accumulating that the ringdown signal is fairly universal even for nonlinear perturbations. For example, various numerical-relativity simulations of compact binary coalescences, both for vacuum and nonvacuum systems, have clearly witnessed excitation of unperturbed quasinormal modes in dynamical processes (see, e.g., Refs. [25,26], for reviews). This prediction is confirmed to large extent by a lot of binary-black-hole observations [27]. These facts strongly suggest that the ringdown signals from a perturbed black hole spacetime do not deviate nonperturbatively from those from the unperturbed spacetime, even if the quasinormal-mode spectrum is destabilized in a catastrophic manner. Stated differently, observable ringdown signals may not necessarily be dictated by quasinormal-mode spectra (see also Ref. [28]), even though they actually are for unperturbed Schwarzschild and Kerr spacetimes.

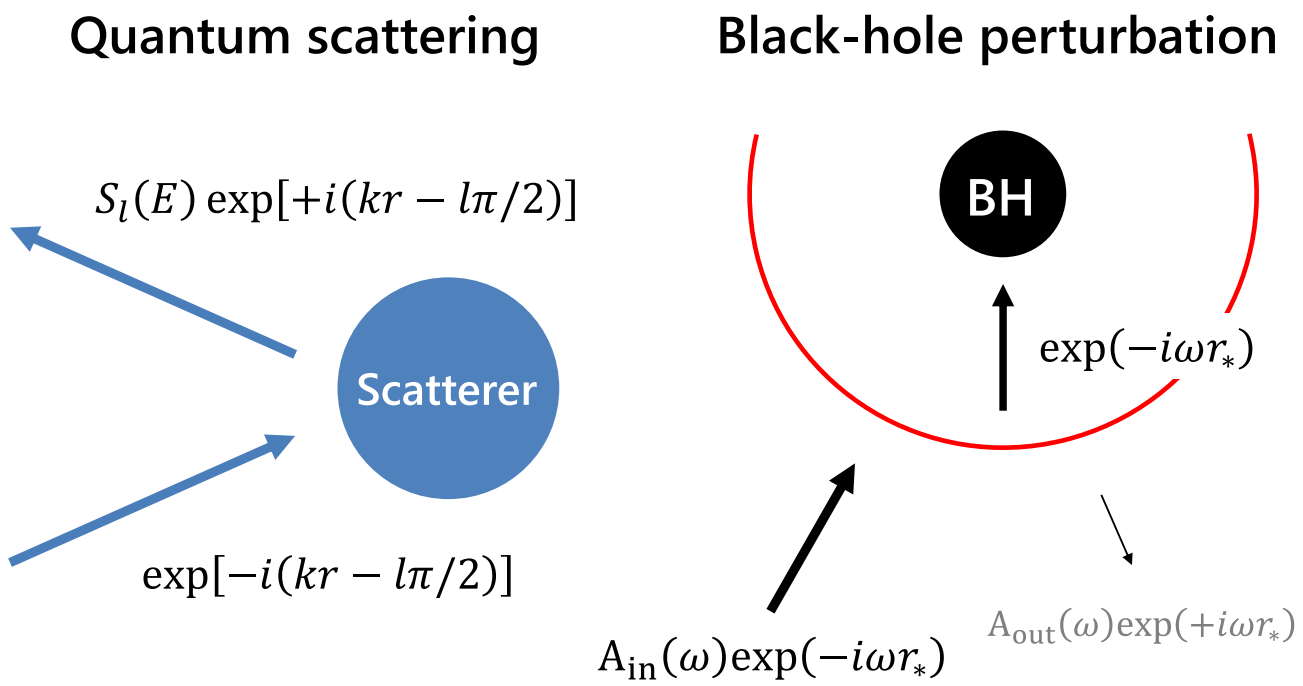

FIG. 1. Schematic figure showing the correspondence between the quantum scattering and the black hole perturbation. In the quantum scattering, we usually consider incident waves with the unit amplitude and scattered waves with the (complex) amplitude $S_l(E)$, and the poles of $S_l(E)$ give us information about the resonance (see, e.g., Ref. [30]). In this study on the black hole perturbation, we consider ingoing waves with the (complex) amplitude $A_{\rm in}(\omega)$ and downgoing-wave components with the unit amplitude, and the zeroes of $A_{\rm in}(\omega)$ or equivalently the poles of $1/A_{\rm in}(\omega)$ actually give us information about the quasinormal modes. The red circle in the right panel is drawn to imply the barrier associated with the Regge-Wheeler potential [31].

For example, fitting of observed ringdown signals against damped sinusoids likely returns complex frequencies not included in the destabilized quasinormal-mode spectra as the strongest component [24].

A probable reason for this irrelevance is that the quasinormal-mode spectrum is defined merely as a result of analytic continuation of the relevant Green's function in terms of the frequency. Mathematically, quasinormal modes are defined as the poles on the complex frequency plane of the Green's function satisfying outgoing (at null infinity) and downgoing (at the event horizon) boundary conditions. Meanwhile, the realistic signal should be decomposed into real-frequency modes by the Fourier transformation. Thus, it is natural to expect that information governing the ringdown signals, which are likely to be tightly related to the poles in the unperturbed black-hole spacetime, is imprinted also in the real-frequency Green's function (see also Ref. [29] for real-frequency analysis of ringdown and echo signals from exotic compact objects). In particular, the fundamental mode, i.e., the quasinormal-mode pole closest to the real axis, should have a decisive impact.

In this study, we investigate the scattering of gravitational waves in black hole spacetimes to demonstrate that distant perturbations to the potential hardly destabilize observable ringdown signals mainly characterized by the unperturbed fundamental mode as anticipated above. As an alternative to the poles on the complex frequency plane, we propose that the phase shift defined from the transmission amplitude of the ingoing waves enables us to infer the properties of unperturbed quasinormal modes in an approximate but stable manner. This tool is taken from the resonance in quantum systems, and the correspondence assumed here is sketched in Fig. 1 (see Sec. II C for detailed discussions). In Sec. II, by solving the time evolution of a Gaussian wave packet, we check that the ringdown signal is stable even under perturbations that destabilize the quasinormal-mode frequency of the fundamental mode. Then, we explain our method to extract useful information from the real-frequency scattering problem. By analyzing a toy model in Sec. III, we first explain how the spectral instability is relevant only for complex frequencies required by analytic continuation and next verify the utility of the phase shift as a real-frequency indicator of dominant modes in the ringdown signal. Equipped with this tool, we return to Schwarzschild black holes and their perturbations in Sec. IV. Section V is devoted to a summary and discussions.

Throughout this paper, we adopt the geometric unit in which $G = c = 1$, where G and c are the gravitational constant and the speed of light, respectively. The mass of the black hole is denoted by M. The Fourier transformation is performed with the convention that

$$f(t) = \int_{-\infty}^{\infty} \tilde{f}(\omega) e^{-i\omega t}\, d\omega. \tag{1}$$

The complex quasinormal-mode frequency is decomposed into the oscillation frequency ω_R and the decay width Γ by $\omega = \omega_R - i\Gamma/2$.

II. STABILITY OF RINGDOWN SIGNALS UNDER SPECTRAL INSTABILITY

To set the stage for this study, we first show that the ringdown signals in the Schwarzschild spacetime associated with the scattering of a Gaussian wave packet is stable under perturbations of the effective potential even if the fundamental mode is destabilized [18] (but see also Ref. [32] for possible alternative definitions of stability in terms of different norms). The significant difference is observed only as late-time excitation of echoes between the primary potential barrier and the perturbation. A similar analysis has recently been made in Ref. [24] for slightly different perturbations, and our results seem consistent with theirs qualitatively. This analysis motivates us to search for the signature of unperturbed quasinormal modes, particularly the fundamental mode, from real-frequency solutions of the scattering problem.

A. Setup

Time evolution of linear waves represented by ϕ around a black hole is governed by hyperbolic equations with effective potentials. Specifically, after spherical harmonic decomposition (whose indices are suppressed here for ease of notation), governing equations reduce to (see, e.g., Ref. [33] for comprehensive reviews)

$$\frac{\partial^2 \phi}{\partial t^2} = \frac{\partial^2 \phi}{\partial r_*^2} - V(r_*)\phi(t, r_*), \tag{2}$$

where $r_* := r + 2M \ln(r/2M - 1) + R_*$ is the tortoise coordinate, and V is the effective potential. Here, for later convenience, we intentionally keep an integration constant R_* in the tortoise coordinate defined by $dr_*/dr = 1/(1 - 2M/r)$ for the Schwarzschild spacetime. Unless otherwise stated, we set $R_* = 0$.

Throughout this article, we focus on the $l = 2$ mode of axial gravitational waves, for which the unperturbed effective potential is given by the so-called Regge-Wheeler potential [31],

$$V_{RW}(r_*) := \left(1 - \frac{2M}{r}\right)\left(\frac{l(l+1)}{r^2} - \frac{6M}{r^3}\right). \tag{3}$$

On another front, the polar gravitational waves obey Eq. (2) with the so-called Zerilli potential [34], which is known to be isospectral with the Regge-Wheeler potential [35]. Vector and scalar waves also obey the same equation with similar potentials. Thus, we expect that the analysis of this study applies to fields of any parity and spins, at least qualitatively.

The quasinormal-mode spectrum including the fundamental mode is reported to be unstable when the potential is augmented by a bump modeled by the Pöschl-Teller form [18],

$$V(r_*) = V_{RW}(r_*) + V_{PT}(r_*; \epsilon, b), \tag{4}$$

$$V_{PT}(r_*; \epsilon, b) := \frac{\epsilon}{(2M)^2 \cosh^2[(r_* - b)/(2M)]}, \tag{5}$$

for sufficiently large values of b and/or ϵ.[36] In this study, we fix $\epsilon = 10^{-3}$, for which the fundamental mode is reported to be destabilized if $b \gtrsim 50M$. We checked that the value of ϵ only determines the scale of the results presented in this study unless it becomes $\sim\mathcal{O}(1)$.

B. Time evolution

To demonstrate that the ringdown signal is stable until the late-time modes are excited, we numerically simulate scattering problems for Eq. (2) with both the Regge-Wheeler potential of Eq. (3) and that perturbed by a Pöschl-Teller bump of Eq. (5) adopting $b = 100M$. The initial data are chosen to be $\phi(t = 0) = 0$ and the time derivative in the form of a Gaussian wave packet,

$$\frac{\partial \phi(t=0)}{\partial t} = \exp\left[-\left(\frac{r_* - r_{*,0}}{2M}\right)^2\right], \tag{6}$$

where $r_{*,0} = -50M$ or $50M$. Essentially the same initial data are adopted in Ref. [23] for investigating the scattering by double rectangular barriers (see also Sec. III below), and we have reproduced their results with reasonable accuracy. The evolved fields are extracted at a finite distance of $r_{*,\mathrm{ext}} = 250M$. The boundaries of our computational domains are located at sufficiently large distances so that numerical reflections do not affect the results shown below.

Figure 2 shows the time evolution of an initial Gaussian wave packet in the Regge-Wheeler potential and that perturbed by a Pöschl-Teller bump. The left panel depicts the scattering of a wave packet initiated at $r_{*,0} = -50M$, and this case corresponds to outward propagation from the inside of the potential peak. It is obvious that the ringdown signals, i.e., the time evolution of the field characterized by exponential damping, are essentially unchanged under perturbations until the echo signal arrives after $\sim 2b = 200M$ from the direct signal. These features agree with those found in the analysis of double rectangular barriers [23] and the Regge-Wheeler potential perturbed by a Gaussian bump [24].

The right panel of Fig. 2 shows the scattering of a wave packet initiated at $r_{*,0} = 50M$, which corresponds to the middle of the main peak and the perturbative bump.

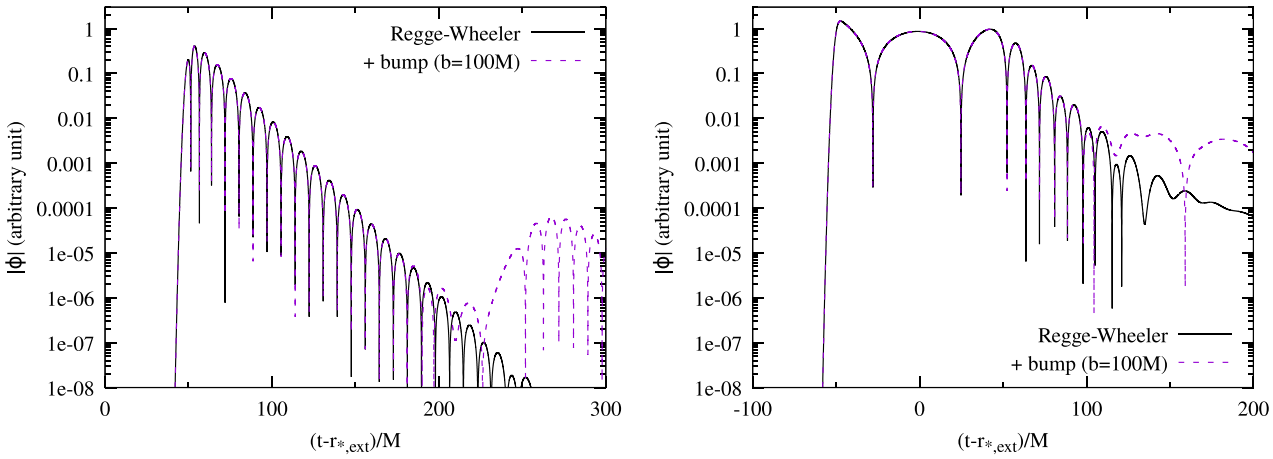

FIG. 2. Time evolution of a Gaussian wave packet in the Regge-Wheeler potential (black solid) and that perturbed by a Pöschl-Teller bump (purple dashed). The Pöschl-Teller bump is located at $b = 100M$ with the amplitude of $\epsilon = 10^{-3}$, with which the fundamental mode is destabilized [18]. The Gaussian wave packets are initially located at $r_{*,0} = -50M$ and $r_{*,0} = 50M$ for the left and right panels, respectively. The origin of the time is chosen to account for the retardation at the extraction radius of $r_{*,\mathrm{ext}} = 250M$. The power-law tail is also observed at $t - r_{*,\mathrm{ext}} \gtrsim 150M$ for the Regge-Wheeler potential with $r_{*,0} = 50M$ [37].

This choice of the initial location enhances the echo signal via the presence of low-frequency components outside the main peak, which can be easily reflected back and forth between the two potential barriers, from the beginning [23,38]. In the case of the right panel, after the direct arrival of a precursor signal at $t - r_{*,\mathrm{ext}} \sim -50M$, the ringdown signal sets in at $\sim 50M$ due to the reflection from the Regge-Wheeler potential. Although the echo signal begins to be dominant as early as $\sim 100M$ for the perturbed spacetime, we can still observe the ringdown signal, whose oscillation frequency and decay width are essentially unchanged from the unperturbed values.

C. Where have the quasinormal modes gone?

Through the case studies shown in Fig. 2, we may safely conclude that the dominant part of the ringdown signal remains stable despite destabilization of the quasinormal-mode spectra. This suggests that *bona fide* quasinormal modes defined as the poles of the Green's function on the complex frequency plane may not always be useful for characterizing observable signatures. A possible alternative may be to rely on Wentzel-Kramers-Brillouin (WKB) and/or similar methods for deriving approximate quasinormal-mode spectra [39–42]. However, this returns the same spectra as the unperturbed case in a trivial manner, unless the potential is expanded to extremely high orders. We would like to develop a method for approximately but stably inferring unperturbed quasinormal modes, which are likely to characterize dominant ringdown signals, and also for extracting influences of perturbations, which are likely to introduce echo signals, simultaneously. Time-domain analysis like Fig. 2 and that presented in Refs. [19,24] is not fully satisfactory, because the results may depend crucially on the initial condition.

The key consideration is that the observable ringdown signals in the time domain should be determined by the Green's function on the real axis of the frequency, irrespective of whether they are evolved from initial data or sourced by matter. In the remainder of this article, we investigate scattering problems in the frequency domain. The Fourier component of the field is governed by

$$\frac{\mathrm{d}^2\tilde{\phi}}{\mathrm{d}r_*^2} + [\omega^2 - V(r_*)]\tilde{\phi} = 0. \tag{7}$$

General solutions of this equation are asymptotically given by a superposition of plane waves, $e^{\pm i\omega r_*}$. We focus on the "in" solution that satisfies purely downgoing boundary condition at the horizon and hence, behaves asymptotically as

$$\tilde{\phi}_{\mathrm{in}}(r_*) = \begin{cases} e^{-i\omega r_*} & (r_* \to -\infty) \\ A_{\mathrm{in}} e^{-i\omega r_*} + A_{\mathrm{out}} e^{+i\omega r_*} & (r_* \to +\infty) \end{cases}, \tag{8}$$

because it plays a central role in determining observable signals at null infinity. The Green's function with downgoing (at the horizon) and outgoing (at null infinity) boundary conditions is inversely proportional to the Wronskian of corresponding homogeneous solutions, which reduces to

$$W = 2i\omega A_{\mathrm{in}}, \tag{9}$$

under the normalization of Eq. (8) and the similar one for the "up" solution that satisfies purely outgoing boundary condition at null infinity. Quasinormal modes are defined by zeroes of $A_{\mathrm{in}}(\omega)$, which are equivalent to the poles of the

Green's function, and they never occur on the real axis due to the flux conservation.

The fact that the zeroes of $A_{\rm in}(\omega)$ define the quasinormal modes is reminiscent of the fact that the poles of the S matrix define the resonance in quantum systems (see, e.g., Sec. 13 of Ref. [30]). Let us recall the latter problem. For the quantum scattering of a particle with mass μ by a spherically symmetric potential, the radial wave function $R_l(r)$ for the l mode is given by a spherical Bessel function. Its asymptotic form is

$$R_l(r\to\infty)\propto e^{-{\rm i}(kr-l\pi/2)}-S_l(E)e^{+{\rm i}(kr+l\pi/2)}, \quad (10)$$

where E is the energy of the particle and $k^2 \coloneqq E/(2\hbar^2\mu)$. As depicted in the left panel of Fig. 1, the first and second terms correspond to the incident and scattered waves, respectively. If the scattering is elastic, the unitarity ensures that the S matrix has the unit amplitude, so that we may write $S_l(E)=\exp[2{\rm i}\delta_l(E)]$ in terms of the (real) phase shift $\delta_l(E)$. Meanwhile, the resonance is mathematically defined on the analytically continued complex energy plane as the pole $E=E_{\rm res}\coloneqq E_{\rm R}-{\rm i}\Gamma_{\rm res}/2$ of the S matrix. Then, the S matrix on the real axis is expected to behave as

$$S_l(E)=e^{2{\rm i}\delta_l(E)}\approx e^{2{\rm i}\delta_{{\rm BG},l}(E)}\frac{E-E^*_{\rm res}}{E-E_{\rm res}} \quad (11)$$

$$=e^{2{\rm i}\delta_{{\rm BG},l}(E)}\frac{E-E_{\rm R}-{\rm i}\Gamma_{\rm res}/2}{E-E_{\rm R}+{\rm i}\Gamma_{\rm res}/2}, \quad (12)$$

where $\delta_{{\rm BG},l}(E)$ is the so-called background phase shift and is expected to be a slowly varying function of E. We stress that the derivative of the phase shift behaves like a Lorentzian function (see, e.g., Sec. 11.4 of Ref. [43]),

$$\frac{{\rm d}\delta_l}{{\rm d}E}\approx\frac{\Gamma_{\rm res}/2}{(E-E_{\rm R})^2+(\Gamma_{\rm res}/2)^2}+\frac{{\rm d}\delta_{{\rm BG},l}}{{\rm d}E}. \quad (13)$$

This quantity serves as a tool to extract the values of $E_{\rm R}$ and $\Gamma_{\rm res}$ via the location of a peak and the full-width-half-maximum (FWHM), respectively, from the real-energy wave function.

To apply this established tool in quantum mechanics to quasinormal modes of black holes as a novel technique (see Refs. [44–48] for related work), we assign ingoing (from null infinity) and downgoing (to the horizon) waves, respectively, the roles of the incident and scattered waves in quantum mechanics [49]. As schematically presented in the right panel of Fig. 1, this identification allows us to investigate $A_{\rm in}(\omega)$ in a similar manner to the Jost function used for defining the S matrix. Hereafter, we occasionally call $1/A_{\rm in}(\omega)$ the (complex) transmission amplitude [50]. Because $A_{\rm in}(\omega)$ vanishes at the complex quasinormal-mode frequency, we expect it to behave near the zero as

$$A_{\rm in}(\omega)\approx\hat{A}_{\rm in}(\omega)\times(\omega-\omega_{\rm R}+{\rm i}\Gamma/2), \quad (14)$$

where $\hat{A}_{\rm in}(\omega)$ is a slowly varying and finite function of ω. Although the transmission amplitude is not unitary and $|A_{\rm in}(\omega)|$ is strictly larger than unity on the real axis in our problem, this approximation derives a manifestly unitary expression,

$$\frac{A_{\rm in}(\omega)^2}{|A_{\rm in}(\omega)|^2}\approx e^{-2{\rm i}\delta_{\rm BG}(\omega)}\frac{\omega-\omega_{\rm R}+{\rm i}\Gamma/2}{\omega-\omega_{\rm R}-{\rm i}\Gamma/2}, \quad (15)$$

$$e^{-2{\rm i}\delta_{\rm BG}(\omega)}\coloneqq\frac{\hat{A}_{\rm in}(\omega)}{\hat{A}^*_{\rm in}(\omega)}, \quad (16)$$

on the real axis. Thus, by defining the phase shift of the transmission amplitude as

$$e^{-{\rm i}\delta(\omega)}=\frac{A_{\rm in}(\omega)}{|A_{\rm in}(\omega)|}, \quad (17)$$

we arrive at the tool to extract quasinormal-mode frequency, i.e., the derivative of the phase shift,

$$\frac{{\rm d}\delta}{{\rm d}\omega}\approx\frac{\Gamma/2}{(\omega-\omega_{\rm R})^2+(\Gamma/2)^2}+\frac{{\rm d}\delta_{\rm BG}}{{\rm d}\omega}. \quad (18)$$

Indeed, this procedure is similar to the definition of the S matrix and the phase shift from the Jost function, while, unlike the case of the quantum scattering, $A_{\rm out}(\omega)$ is not equivalent to $A_{\rm in}(-\omega)$ and is not utilized here. If this phase shift enables us to extract, at least approximately, the oscillation frequency and the decay width of quasinormal modes for the unperturbed potential, the same information may also be inferred from the phase shift for the perturbed potential, taking the stability of ringdown signals into account.

It should be remarked that our primary interest is in the functional structure of $A_{\rm in}(\omega)$ such as zeroes and poles, and whether the component is physically scattered or not is irrelevant here. The S matrix in quantum mechanics is referred only to explain the idea behind our method. If we take the word "scattering" literally, the reflected, outgoing component is naturally regarded as the scattered component. Actually, a lot of previous work on the scattering and quasinormal modes for the black hole spacetimes have been performed based on this natural identification (see, e.g., Ref. [51] and references therein for reviews of early work on the scattering problem). In this study, we neglect the outgoing component, because the relevant Green's function is determined entirely by $A_{\rm in}(\omega)$ of the ingoing component.

In fact, $A_{\rm out}$ has some drawbacks for defining the phase shift. First of all, the phase of $A_{\rm out}$ depends on the choice of the tortoise coordinate via R_*, while its magnitude for the real frequency is simply given by $|A_{\rm out}|^2=|A_{\rm in}|^2-1$ via the flux conservation. Still, the derivative of $\arg(A_{\rm out})$ may

contain invariant information, and actually, the derivative of the phase shift defined from the scattering amplitude $A_{\rm out}/A_{\rm in}$ appears to work in a similar manner to the one defined from $A_{\rm in}$ in principle. However, from the technical point of view, the numerical accuracy tends to be degraded at high frequencies, because $|A_{\rm out}|$ becomes small due to the very weak reflection by the potential. Additionally, the weak reflection at high frequencies makes $A_{\rm out}$ fairly sensitive to perturbations, so that its phase changes rapidly in a manner not necessarily related to the quasinormal modes. Hence, we focus on the phase shift defined from $A_{\rm in}$ and its derivative in this study.

In the following, we apply the idea developed in this section to the investigation of ringdown signals and their stability in the Schwarzschild spacetime. However, we defer the discussion on the Regge-Wheeler potential and its perturbation to Sec. IV. Instead, we start from investigating a toy model in the next section.

III. TOY MODEL: RECTANGULAR BARRIERS

To identify the cause of quasinormal-mode instability and to test the strategy presented in the previous section, it is instructive to study an analytically solvable toy model consisting of double rectangular barriers. The potential is given by [18,23]

$$V(r_*) = \begin{cases} 0 & (r_* < 0) \\ V_0 & (0 \le r_* < a) \\ 0 & (a \le r_* < b) \\ V_1 & (b \le r_* < b+d) \\ 0 & (b+d \le r_*) \end{cases}. \tag{19}$$

If $V_1 = 0$, this potential reduces to a single rectangular barrier adopted by seminal work of Chandrasekhar and Detweiler [35], and the "in" solution in the form of Eq. (8) satisfies

$$A_{\rm in} = e^{+{\rm i}\omega a}\frac{2\omega k\,\cos(ka) - {\rm i}(k^2+\omega^2)\,\sin(ka)}{2\omega k}, \tag{20}$$

$$A_{\rm out} = e^{-{\rm i}\omega a}\frac{{\rm i}(k^2-\omega^2)\,\sin(ka)}{2\omega k}, \tag{21}$$

where $k^2 := \omega^2 - V_0$. If $V_1 \neq 0$, not necessarily requiring $V_1 \ll V_0$, the solution changes to

$$\begin{aligned} A_{\rm in} = \frac{1}{4\omega^2 kk'}(&\{4\omega^2 kk'\,\cos(ka)\,\cos(k'd) - (\omega^2+k^2)(\omega^2+k'^2)\sin(ka)\,\sin(k'd) \\ &- 2{\rm i}\omega[k(\omega^2+k'^2)\,\cos(ka)\sin(k'd) + k'(\omega^2+k^2)\sin(ka)\cos(k'd)]\}e^{+{\rm i}\omega(a+d)} \\ &+ (\omega^2-k^2)(\omega^2-k'^2)\sin(ka)\sin(k'd)e^{+{\rm i}\omega(2b-a+d)}), \end{aligned} \tag{22}$$

$$\begin{aligned} A_{\rm out} = \frac{1}{4\omega^2 kk'}\{&[(\omega^2+k'^2)\sin(k'd) - 2{\rm i}\omega k'\,\cos(k'd)](\omega^2-k^2)\sin(ka)e^{-{\rm i}\omega(a+d)} \\ &- (\omega^2-k'^2)\,\sin(k'd)[(\omega^2+k^2)\,\sin(ka) + 2{\rm i}\omega k\cos(ka)]e^{-{\rm i}\omega(2b-a+d)}\}, \end{aligned} \tag{23}$$

where $k'^2 := \omega^2 - V_1$.

The real and imaginary parts of $A_{\rm in}$ for both the single and double rectangular barriers are displayed in Fig. 3. In this and the following figures, we specifically adopt $V_0 = (0.4/M)^2$ and $V_0 a = 9/(4M)$ for the primary barrier to mimic the height and the integral of the Regge-Wheeler potential. Parameters of the second barrier is chosen to $b = 100M$, $d = a$, and $V_1 = 10^{-3}/(2M)^2$. We still normalize V and ω by "the mass of the black hole," M as VM^2 and $M\omega$, although it is absent from the problem of rectangular barriers. While the single barrier can be normalized by a with leaving $V_0 a^2$ as the only parameter, introducing M seems equally useful for the case of multiple barriers.

Figure 3 indicates that $A_{\rm in}$ for the real frequency does not change appreciably even in the presence of the second barrier except for the low-frequency regime $M\omega \lesssim \sqrt{V_1 M^2} = 0.016$. This comparison strongly indicates the stability of the ringdown signal. Indeed, while the perturbative second barrier also destabilizes the quasinormal-mode spectrum [18], the dominant ringdown signal resulting from scattering is stably characterized by the fundamental mode of the unperturbed potential [23].

A. Reason for the quasinormal-mode instability

This toy model indicates that the quasinormal-mode instability is relevant only for complex frequencies required by analytic continuation of $A_{\rm in}$ given by Eq. (22), specifically the factor $e^{2{\rm i}\omega b}$ appearing in the last line. On the one hand, $A_{\rm in}$, the Wronskian, and the Green's function are modified only on the order of V_1/V_0 for $\omega \gg \sqrt{V_1}$, as far as the frequency is real. Thus, the ringdown signals are also kept unchanged within the order of perturbations, V_1/V_0.

On the other hand, the negative imaginary part of the frequency, $\Gamma > 0$, is the essential ingredient of the quasinormal modes. They introduce a contribution in the form of $e^{\Gamma b}$, which grows exponentially as the value of b increases;

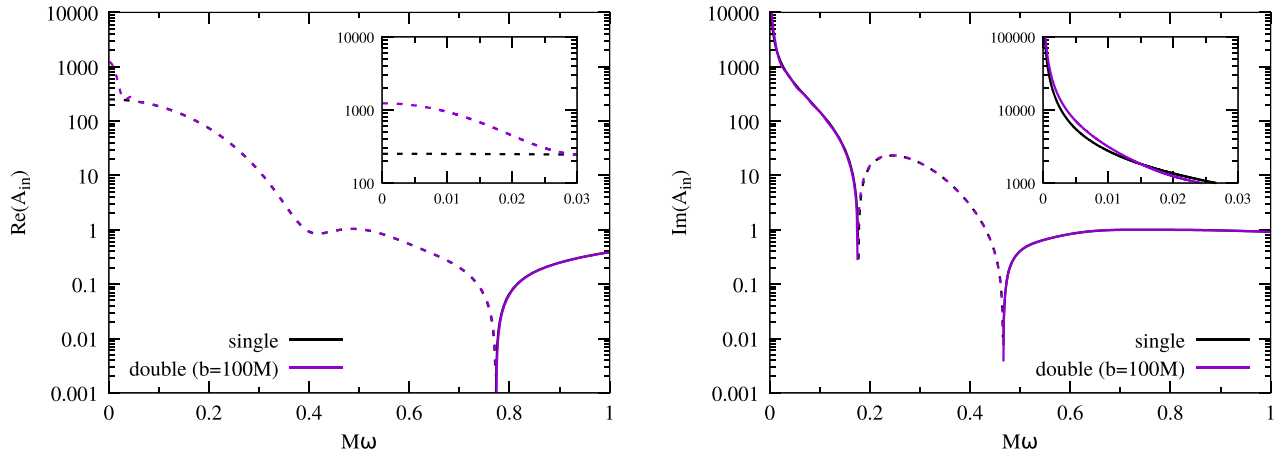

FIG. 3. Real (left) and imaginary (right) parts of $A_{\rm in}$ for the single and double rectangular barriers. The solid and dashed curves denote the positive and negative values, respectively. We set the parameters of the primary barrier to $V_0 = (0.4/M)^2$ and $a = 9/(4MV_0)$ aiming at mimicking the height and the integral of the Regge-Wheeler potential. The second barrier is given by $b = 100M$, $d = a$, and $V_1 = 10^{-3}/(2M)^2$. Curves in both panels are mostly indistinguishable for $M\omega \gtrsim \sqrt{V_1 M^2} = 0.016$ as depicted in the insets.

i.e., the second barrier is moved to a large distance. This exponential dependence is responsible for the spectral instability of quasinormal modes on the complex frequency plane (see also discussions in Ref. [52] and Sec. IIIC1 of Ref. [23]). Actually, even for the case of the Regge-Wheeler potential perturbed by a Pöschl-Teller bump, the threshold for the fundamental-mode instability shown in Fig. 2 of Ref. [18] appears to agree reasonably with the dependence of $\epsilon e^{\Gamma b} = \text{const.}$ expected for the impact of the bump. To support this argument, we demonstrate that the same mechanism works for generic two separated potentials in the Appendix.

B. Quasinormal mode from the phase shift

We move to extraction of quasinormal modes from the phase shift of the transmission amplitude, $1/A_{\rm in}$, on the real axis of the frequency. As a preparation, Table I presents the oscillation frequency $\omega_{\rm R}$ and the decay width Γ for a single barrier. They are determined from the zeroes of $A_{\rm in}$ in the complex frequency plane in a usual manner and are also confirmed to characterize the ringdown signals. This table also presents information extracted from the derivative of the phase shift, $\omega_{\rm peak}$ and $\Gamma_{\rm FWHM}$, described below.

TABLE I. Fundamental ($n = 0$) and first two overtone ($n = 1$, 2) modes for the single rectangular barrier with $V_0 = (0.4/M)^2$ and $a = 9/(4MV_0)$, which can be summarized as $V_0 a^2 = 2025/64$. The oscillation frequency and the decay width are presented by a normalized form of $M\omega_{\rm R}$ and $M\Gamma$, respectively. If the corresponding information can directly be extracted from the phase shift of the transmission amplitude $1/A_{\rm in}$, it is also presented as $M\omega_{\rm peak}$ and $M\Gamma_{\rm FWHM}$.

n	$M\omega_{\rm R}$	$M\Gamma$	$M\omega_{\rm peak}$	$M\Gamma_{\rm FWHM}$
0	0.4434	0.06319	0.4442	0.0566
1	0.5689	0.1918	0.5672	N/A
2	0.7458	0.3079	N/A	N/A

The derivative of the phase shift for a single rectangular barrier is given by

$$\frac{d\delta_{\rm s}}{d\omega} := aV_0 \frac{ka[2\omega^2 - V_0 \sin^2(ka)] - 2V_0 \sin(ka)\cos(ka)}{ka[4\omega^2 k^2 + V_0^2 \sin^2(ka)]}. \tag{24}$$

The full expression for the double rectangular barriers does not seem very enlightening. Instead, we show the expression up to the linear order of V_1/ω^2,

$$\frac{d\delta_{\rm d}}{d\omega} := \frac{d\delta_{\rm s}}{d\omega}\left(1 - \frac{V_1 A_1}{A_0}\right) + \frac{V_1 D}{A_0}, \tag{25}$$

where

$$A_0 := 4\omega^4[4\omega^2 k^2 + V_0^2 \sin^2(ka)], \tag{26}$$

$$\begin{aligned} A_1 := {} & 4\omega^2 V_0 \{2\omega k \cos(ka)\cos[\omega(2b - 2a + d)] \\ & - (\omega^2 + k^2)\sin(ka)\sin[\omega(2b - 2a + d)]\} \\ & \times \sin(ka)\sin(\omega d), \end{aligned} \tag{27}$$

$$D := D_o + D_a + D_d + D_b + 2\omega^2 d[4\omega^2 k^2 + V_0^2 \sin^2(ka)], \tag{28}$$

$$\begin{aligned} D_o := {} & 4V_0 \left\{ \frac{\omega^2(\omega^2 + 3k^2)}{k} \cos(ka)\sin[\omega(2b - 2a + d)] \right. \\ & \left. + \omega(3\omega^2 + k^2)\sin(ka)\cos[\omega(2b - 2a + d)] \right\} \\ & \times \sin(ka)\sin(\omega d), \end{aligned} \tag{29}$$

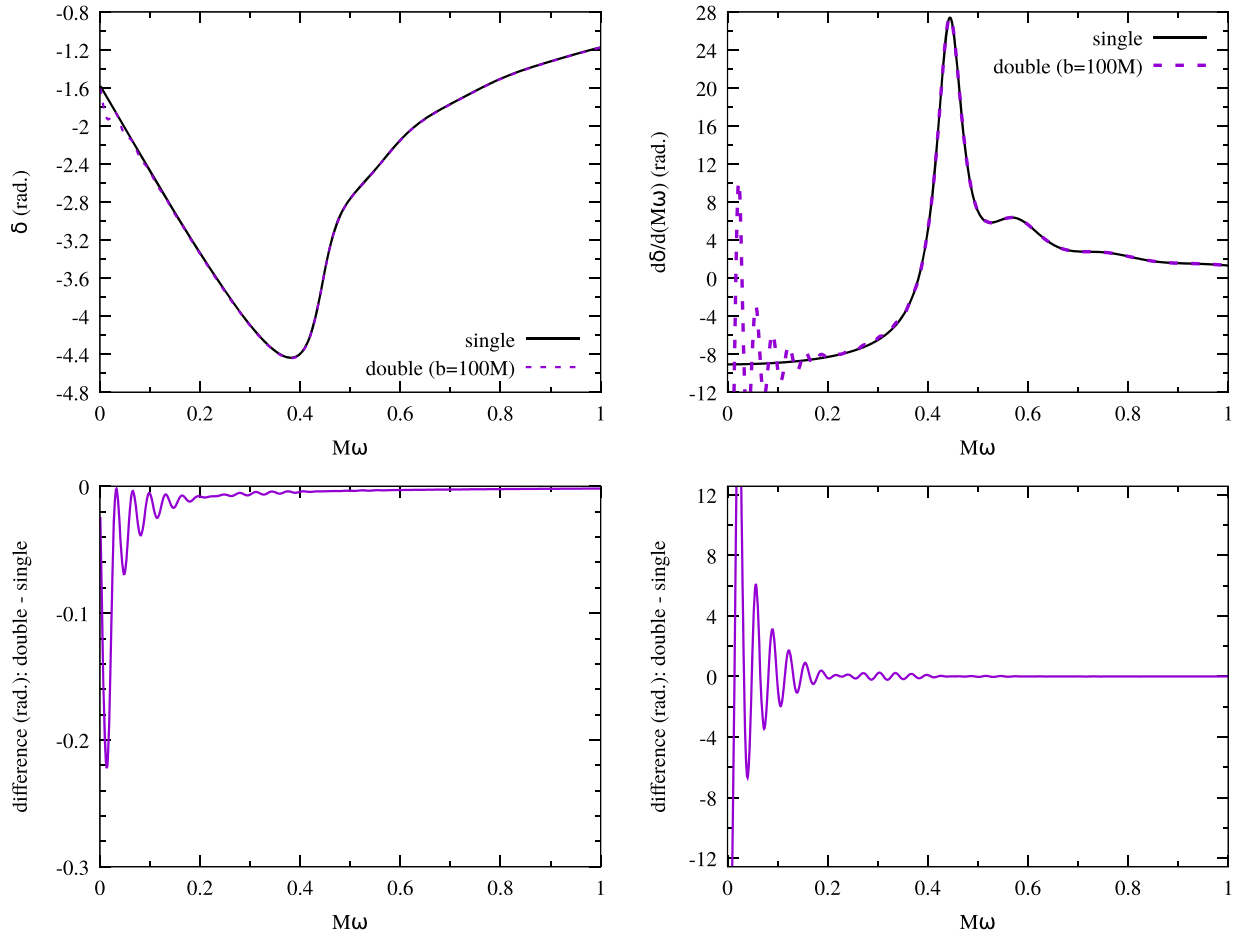

FIG. 4. Phase shift (left) and its derivative with respect to the frequency (right) for the single and double rectangular barriers (top) and their differences (bottom). The parameters of the potential are the same as those adopted in Fig. 3. The primary peak of the derivative is located at $M\omega_{\rm peak} = 0.4442$ with the FWHM being $M\Gamma_{\rm FWHM} = 0.0566$. These values should be compared with $M\omega_{\rm R} = 0.4434$ and $M\Gamma = 0.06319$ for the fundamental mode of a single barrier (see Table I). Another peak is also observed at $M\omega_{\rm peak} = 0.5672$, compared to $M\omega_{\rm R} = 0.5689$ of the first overtone, although the FWHM cannot be extracted.

$$D_a \coloneqq -4V_0\omega^4 a\sin(\omega d)\sin[\omega(2b-2a+d)], \tag{30}$$

$$\begin{aligned} D_d \coloneqq & -2V_0\omega^2 d\{2\omega k\cos(ka)\sin[\omega(2b-2a+d)] \\ & +(\omega^2+k^2)\sin(ka)\cos[\omega(2b-2a+d)]\} \\ & \times\sin(ka)\cos(\omega d), \end{aligned} \tag{31}$$

$$\begin{aligned} D_b \coloneqq & 2V_0\omega^2(2b+d) \\ & \times\{(\omega^2+k^2)\sin(ka)\sin[\omega(2b-2a+d)] \\ & -2\omega k\cos(ka)\cos[\omega(2b-2a+d)]\} \\ & \times\sin(ka)\sin(\omega d). \end{aligned} \tag{32}$$

When the second barrier is located at a large distance, the term D_b with an overall factor $2b+d \sim 2b$ introduces an apparently nonperturbative correction to the derivative of the phase shift with the period in frequency of $\Delta\omega = 2\pi/(2b-2a+d) \sim \pi/b$.

The phase shift and its derivative are shown in Fig. 4 both for the single and double rectangular barriers. First, we focus on the clean case of the single barrier. The derivative of the phase shift clearly exhibits a sharp peak at $M\omega_{\rm peak} = 0.4442$ with the FWHM being $M\Gamma_{\rm FWHM} = 0.0566$ (see Table I). The value of $\omega_{\rm peak}$ agrees with the oscillation frequency $\omega_{\rm R}$ of the fundamental mode within $\approx 0.2\%$. The value of $\Gamma_{\rm FWHM}$ agrees with the decay width Γ of the fundamental mode within $\approx 10\%$. This analysis convinces us that the fundamental mode can approximately be extracted from the phase shift defined from the real-frequency solutions of the scattering problem for the case of a single rectangular barrier.

The deviation in the decay width may be ascribed, at least partially, to contamination by a subdominant peak at $M\omega_{\rm peak} = 0.5672$. This value agrees with the oscillation frequency of the first overtone, $M\omega_{\rm R} = 0.5689$, within $\approx 0.3\%$. Thus, we believe that this subdominant peak is associated with the first overtone, although the FWHM is

no longer available in a straightforward manner. We also see a shoulderlike structure around the oscillation frequency of the second overtone, $M\omega_{\rm R} = 0.7458$, while there is no extremum. Although we have not performed comprehensive analysis, for a larger value of V_0a^2, a larger number of peaks associated with higher overtones become distinguishable. These observations suggest that multiple quasinormal modes may be extracted from $A_{\rm in}$ on the real axis by careful analysis. Indeed, this must obviously be true if the higher overtones contribute to observable ringdown signals [53–56]. It should be cautioned, however, that $\Gamma_{\rm FWHM}$ of the main peak is not larger but smaller than Γ of the fundamental mode for the parameters adopted in this study. This implies that higher overtones are unlikely to be extracted by simply assuming that $d\delta/d\omega$ is given by a sum of multiple peaks. Extraction of multiple quasinormal modes is our ongoing project, and the result will be presented elsewhere.

Remarkably, even if the second barrier is turned on and the quasinormal-mode spectrum is destabilized [18], as shown in Fig. 4, the phase shift retains information about the unperturbed quasinormal modes [57]. The second barrier produces modulation in the phase shift δ itself only on the order of V_1/V_0 for the frequency around the unperturbed quasinormal modes. While the modulation is enhanced by a factor of $\sim 2b/M$ due to the differentiation, the profile of $d\delta/d\omega$ still recovers the unperturbed peaks once averaged over the frequency range wider than $\Delta\omega \sim \pi/b$ [58]. This feature explains why the initial stage of the ringdown signal in the perturbed spacetime is characterized by the unperturbed quasinormal modes even if the poles are destabilized on the complex frequency plane. Here, we should recall that the fine resolution in the frequency domain becomes relevant only when we have sufficiently long time-domain data. Thus, the averaging over the frequency is naturally introduced when we focus on a short time scale of $\lesssim 2b$ (see also Refs. [19,23,24] for relevant discussions).

For the case of double barriers, quasinormal modes associated with the late-time echo signal may also be imprinted in the phase shift and its derivative. The amplitude of the modulation in the phase shift grows as the frequency decreases. Together with the enhancement by a factor of $\sim 2b/M$, this dependence results in formation of equidistant narrow peaks at low frequencies for the derivative of the phase shift. The separation of $\Delta\omega \sim \pi/b$ between the maxima of these peaks represents the travel time between the two barriers, and the narrow widths may be consistent with long lifetimes. Thus, these peaks may correspond to quasinormal modes associated with the echoes between two barriers. However, because the peaks in $d\delta/d\omega$ appear both as maxima and minima and its central value is displaced from zero to $\approx -(4\text{–}5)$ rad, physical interpretations of these peaks are not as straightforward as those of the main peak for the unperturbed fundamental mode (see also Sec. IV).

Before concluding this section, we mention that the magnitude of the transmission amplitude on the real axis also reflects information about the quasinormal modes, although not as clearly as the phase shift and its derivative do. Figure 5 shows the magnitude of $A_{\rm in}$ in terms of $|A_{\rm in}|^2 - 1 = |A_{\rm out}|^2$ and $1/|W| = 1/|2\omega A_{\rm in}|$ as functions of the real frequency. The oscillatory behavior of the former is characteristic of the exactly rectangular potential, which becomes transparent at discrete frequencies satisfying $\sin(ka) = 0$. The inverse of the Wronskian becomes large at these specific frequencies as found in the right panel, and the overall features are similar to $d\delta/d\omega$ shown in the right panel of Fig. 4. Still, the peak frequency agrees only within $\approx 5\%$ with the oscillation frequency of the fundamental mode, compared to $\approx 0.2\%$ for the phase shift. Moreover, it is not obvious how to extract decay widths from the broad profile. Thus, we tentatively conclude that the phase is more useful than the magnitude for extracting information about the ringdown signal. However, we recall that both the magnitude and phase of $A_{\rm in}$ or W on the real axis are necessary to recover all the information on the complex frequency plane.

IV. PHASE SHIFT FOR SCHWARZSCHILD BLACK HOLES

We come back to our main problem of a Schwarzschild black hole and its perturbation. Let us consider the potential given by Eq. (4), i.e., the Regge-Wheeler potential augmented by a small Pöschl-Teller bump. Real-frequency "in" solutions in the form of Eq. (8) are derived numerically for $b = 100M$ and $200M$, aiming at checking the dependence on b, as well as for the unperturbed Regge-Wheeler potential. The real and imaginary parts of $A_{\rm in}$ are shown in Fig. 6. As we have noticed in Sec. II, a perturbative Pöschl-Teller bump modifies $A_{\rm in}$ only in a perturbative manner except for the low frequency of $M\omega \lesssim \sqrt{\epsilon}/2 = 0.016$. In the following, we present information about quasinormal modes contained in $A_{\rm in}$ along the line presented in Sec. III B for the rectangular barriers. We remind that the fundamental mode of the Regge-Wheeler (and also Zerilli) potential has the oscillation frequency of $M\omega_{\rm R} = 0.3737$ and the decay width of $M\Gamma = 0.1779$ (see, e.g., Ref. [59]).

Figure 7 shows the phase shift and its derivative with respect to the frequency. Comparisons with the results for the single rectangular barrier presented in Fig. 4 reveal that the phase shift for the Regge-Wheeler potential exhibits a smooth structure without a clear second peak. This is naturally understood by regarding the Regge-Wheeler potential as a sequence of rectangular barriers with various widths and heights (see also Ref. [20]). Another way of explaining this smoothness is that the real parts of the overtone modes are closer to the fundamental mode than in the case of the single rectangular barrier. The single peak in $d\delta/d\omega$ of Fig. 7 is characterized by $M\omega_{\rm peak} = 0.3758$ and

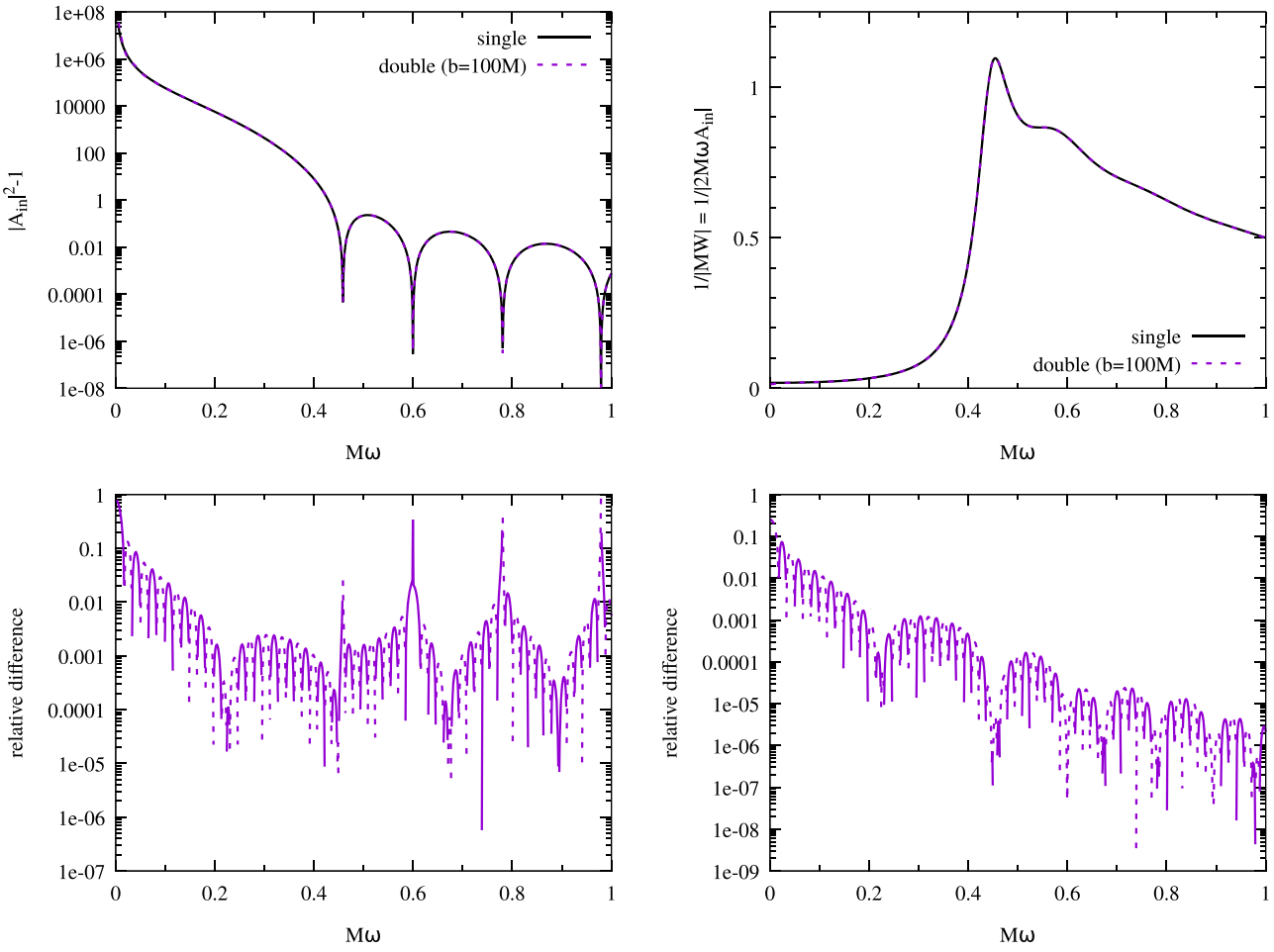

FIG. 5. Magnitude of the transmission amplitude in the form of $|A_{\rm in}|^2 - 1 = |A_{\rm out}|^2$ (left) and of the inverse of Wronskian, $1/|W| = 1/|2\omega A_{\rm in}|$ (right) for the single and double rectangular barriers (top) and their relative differences (bottom). The parameters of the potential are the same as those adopted in Fig. 3. The solid and dashed curves in the bottom panel represent positive and negative values, respectively, which indicate the excess and the deficit for the double barriers, respectively. The relative difference is enhanced for $|A_{\rm in}|^2 - 1 \approx 0$ in the left panel.

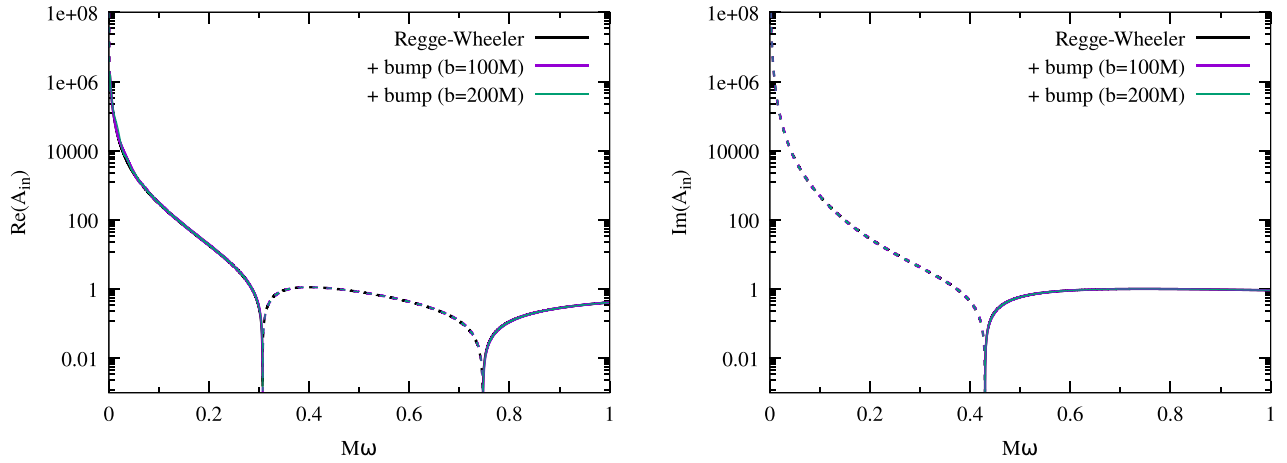

FIG. 6. Real (left) and imaginary (right) parts of $A_{\rm in}$ for the Regge-Wheeler potential (black) and that perturbed by a Pöschl-Teller bump at $b = 100M$ (purple) or $200M$ (green). The solid and dashed curves denote the positive and negative values, respectively. The magnitude of the bump is $\epsilon = 10^{-3}$. All the curves are mostly indistinguishable for $M\omega \gtrsim \sqrt{\epsilon}/2 = 0.016$.

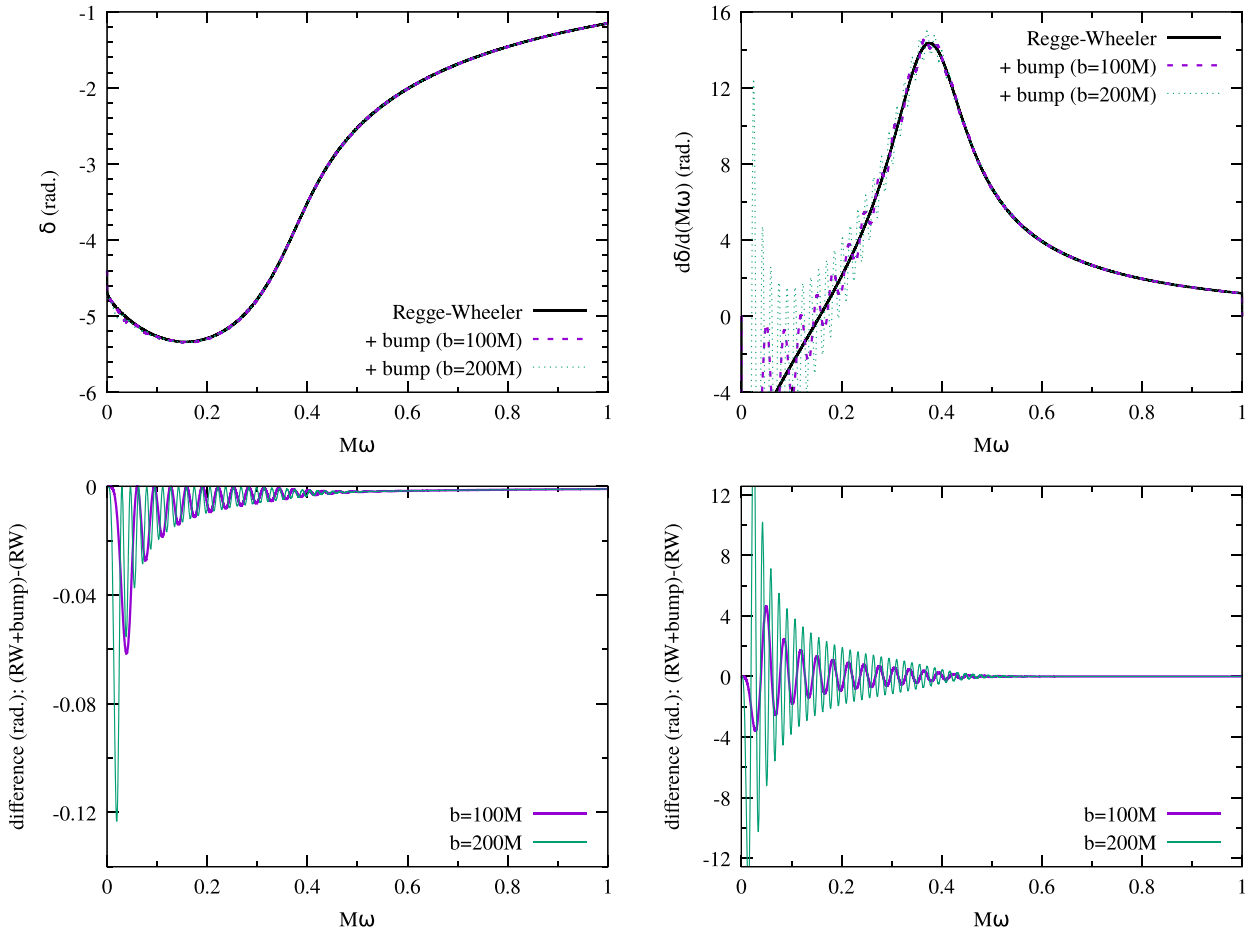

FIG. 7. Top: Phase shift (left) and its derivative with respect to the frequency (right) for the Regge-Wheeler potential (black solid) and that perturbed by a Pöschl-Teller bump at $b = 100M$ (purple dashed) or $200M$ (green dotted). The magnitude of the bump is $\epsilon = 10^{-3}$. For the Regge-Wheeler potential, the derivative peaks at $M\omega_{\rm peak} \approx 0.3758$ with the FWHM being $M\Gamma_{\rm FWHM} \approx 0.211$. These values should be compared with $M\omega_{\rm R} = 0.3737$ and $M\Gamma = 0.1779$ of the fundamental mode (see, e.g., Ref. [59]). The modulation seen for the perturbed potential has a period of $\Delta\omega \approx \pi/b$, and its amplitude grows as the frequency decreases. Bottom: Differences between the quantities for the Regge-Wheeler potential and that perturbed by a Pöschl-Teller bump.

$M\Gamma_{\rm FWHM} = 0.211$, which agrees with the oscillation frequency and the decay width of the fundamental mode of the Schwarzschild black hole within ≈0.6% and ≈20%, respectively. The level of agreement is comparable but worse by a factor of 2–3 than the case of a single rectangular barrier. This may again be ascribed to contamination by higher overtones. Specifically, because the oscillation frequency of the first overtone is lower only by ≈7% than that of the fundamental mode [59], multiple poles are likely to be contributing to the apparently single peak. This interpretation may be supported by the fact that no isolated peak is found for higher overtones.

The derivative of the phase shift allows us to understand the relation between the quasinormal modes and the ringdown signal in an intuitive manner. In quantum mechanics, the derivative of the phase shift has been recognized to describe the time delay in the scattering process of a wave with a given frequency [60]. Because a wave packet is formed at the frequency around which the time delay is nearly stationary, the observable ringdown signal is naturally characterized by the peak frequency of the derivative of the phase shift. This interpretation appears consistent with the conventional understanding that the quasinormal mode is the leakage of waves transiently trapped around the light ring [5]. In turn, this assessment suggests that the derivative of the phase shift is directly related to observable ringdown signals even if the quasinormal-mode spectra are destabilized.

The influence of the Pöschl-Teller bump on the phase shift is only perturbative, confirming the stability of the ringdown signal found in Sec. II. Because the modulation has a period in frequency of $\Delta\omega \sim \pi/b$, the influence on the derivative of the phase shift is enhanced by a factor of $\sim 2b/M$ (see the right panel of Fig. 7). Still, the overall shape of the peak is unchanged around the unperturbed

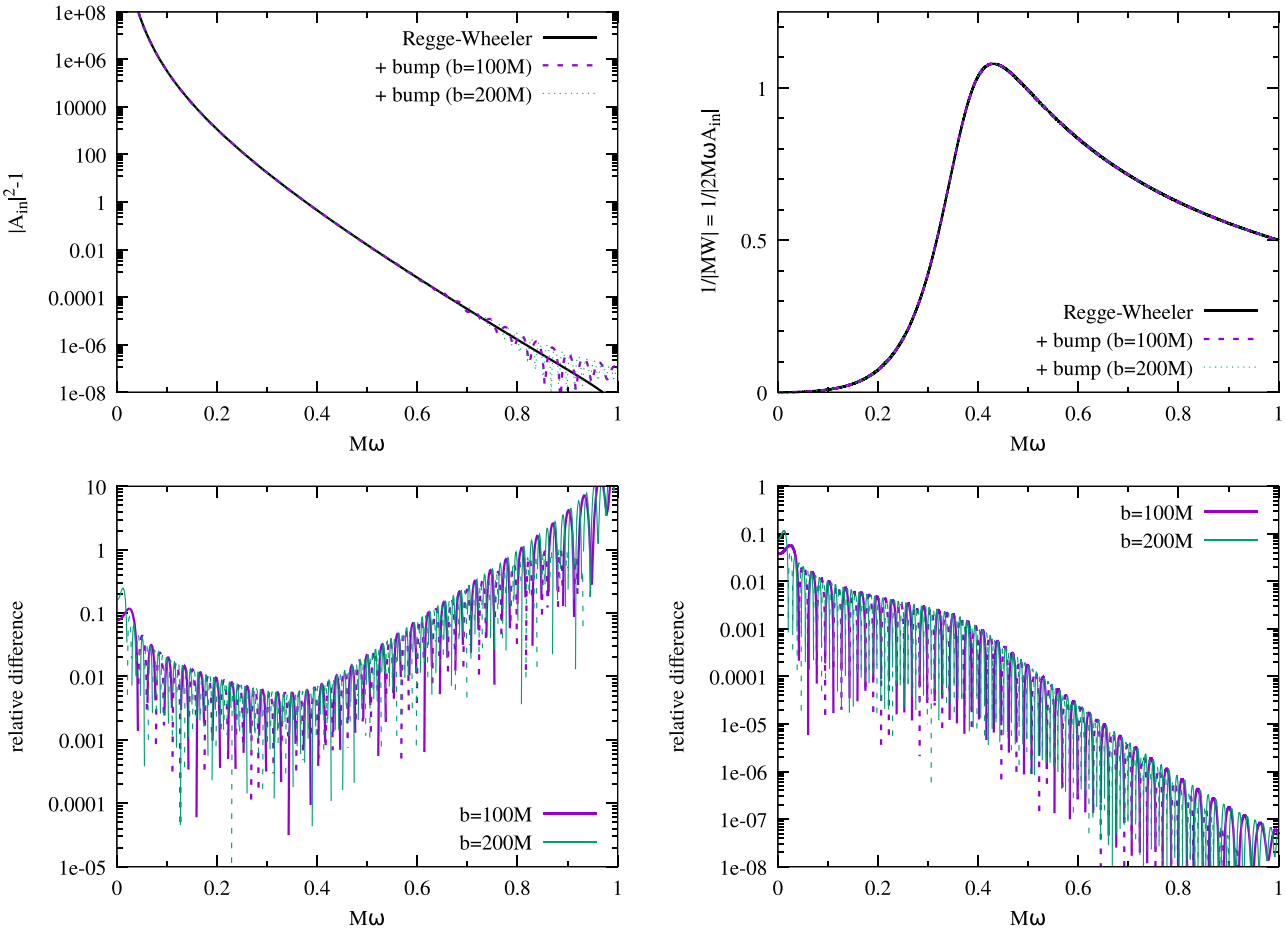

FIG. 8. Top: Magnitude of the transmission amplitude in the form of $|A_{\rm in}|^2 - 1 = |A_{\rm out}|^2$ (left) and of the inverse of Wronskian, $1/|W| = 1/|2\omega A_{\rm in}|$ (right) for the Regge-Wheeler potential (black solid) and that perturbed by a Pöschl-Teller bump at $b = 100M$ (purple dashed) or $200M$ (green dotted). The magnitude of the bump is $\epsilon = 10^{-3}$. Bottom: Relative difference between the quantities for the Regge-Wheeler potential and that perturbed by a Pöschl-Teller bump. The solid and dashed curves denote the positive and negative values, respectively, which indicate the excess and the deficit of values for perturbed potentials, respectively.

fundamental mode, and an appropriate averaging of the phase shift (rather than its derivative) over the frequency will allow us to extract the unperturbed fundamental mode in an approximate but stable manner. Again, this feature should be the explanation for the stability of dominant ringdown signals under the spectral instability of quasinormal modes. At low frequencies, the amplitude of the modulation grows in a similar manner to the case of double rectangular barriers. This growth forms a bunch of peaks in the derivative of the phase shift. These peaks are likely to represent quasinormal modes associated with the echoes between the Regge-Wheeler potential and the perturbative bump.

To sum up, the behavior of the phase shift for the Regge-Wheeler potential with a possible perturbative bump is qualitatively the same as that for the rectangular barriers. A notable difference is the absence of distinguishable subdominant peaks associated with the higher overtones. This may be reasonably explained by the proximity of the poles for the unperturbed Regge-Wheeler potential.

We also present information related to the magnitude of the transmission amplitude in Fig. 8. Differently from the case of rectangular barriers, $|A_{\rm in}|^2 - 1 = |A_{\rm out}|^2$ is a monotonic function except for tiny effects of a perturbative bump. This is a mere repetition of the well-known fact that the reflection and thus, transmission coefficients of the Regge-Wheeler potential are monotonic functions [61]. The magnitude of deviations observed for $M\omega \gtrsim 0.8$ is only on the order of ϵ^2, indicating that the reflection coefficient is modified by filtering due to the Pöschl-Teller bump on this order. The differences in $|A_{\rm in}|^2 - 1$ and $1/|W|$ between the unperturbed and perturbed potentials change its frequency dependence at $M\omega \approx 0.4$, which corresponds to the peak of the Regge-Wheeler potential. The fact that the envelopes of these curves are approximately independent of the value of b is another indication that the location of the perturbative bump does not influence the stability of ringdown signals, although the quasinormal-mode spectrum can be destabilized due to analytic continuation to the complex plane.

Instead, the dependence on b resides in the period of the oscillation, $\sim\pi/b$. While the inverse of the Wronskian seems to contain some information about quasinormal modes in a similar manner to the rectangular barriers shown in Fig. 5, it is not as clear as the phase shift and its derivative do.

V. SUMMARY AND DISCUSSION

We investigated the influence of proposed spectral instability of quasinormal modes on the observable ringdown signal. We find that perturbations to the potential is unlikely to destabilize the ringdown signal, which is rather stably characterized by quasinormal modes in the unperturbed spacetime except for the late-time echo signals. The quasinormal-mode spectra owe their instability to analytic continuation with respect to the frequency. Specifically, a phase factor of the form $e^{2i\omega b}$, with b being the distance between the two potentials, in $A_{\rm in}$ introduces an exponentially growing contribution once the frequency gains a negative imaginary part, which in fact is the essential ingredient of the quasinormal modes.

Quasinormal modes of the unperturbed spacetime can be extracted from real-frequency solutions of the scattering problem via the phase shift defined from the transmission amplitude, $1/A_{\rm in}$ in our notation, even if a perturbation destabilizes the quasinormal-mode spectrum. This approach is motivated by the similarity of quasinormal modes of black holes to resonances in quantum systems. Although this extraction is not as precise as traditional methods such as the continued fraction method [59], the phase shift is advantageous in its immunity to destabilization of *bona fide* quasinormal modes due to the analytic continuation. Rather, quasinormal modes extracted from the phase shift may enable us to characterize observable ringdown signals in an approximate but stable manner. The implication of this method to the observable signal is that the dominant ringdown signal is stably characterized by the unperturbed quasinormal modes even under the spectral instability of quasinormal modes, and the perturbative bump instead excites late-time echo signals, whose amplitude is suppressed accordingly to the smallness of the bump. They agree with and thus reconfirm the results of time evolution.

The analysis in terms of the phase shift may be applicable to a wide range of spacetimes, most importantly the Kerr black hole and its perturbed siblings. Potential difficulties, though not so serious, are how to handle complex potentials associated with the black hole spins [65,66], and transformation that makes the potential real may be preferred [67,68]. It would also be beneficial to perform systematic studies of quasinormal modes in Schwarzschild spacetimes varying the parity, the spin of the field, and the spherical harmonic eigenvalues.

After understanding that the ringdown signal is characterized by information on the real axis, another question arises; why the ringdown signal appears to be represented faithfully by the poles on the complex plane for a simple potential like Regge-Wheeler's one? And, when the quasinormal-mode spectrum is completely destabilized so that the pole of the original fundamental mode disappears [18], how do the remaining poles reproduce the original quasinormal modes in the ringdown signal? It seems that a series of poles generated by perturbations must be conspiring to preserve influence of the original pole, at least of the fundamental mode, on the ringdown signal. This may be accomplished by suitable distributions of the excitation factors [69]. Our current study only considers the frequency of quasinormal modes, and their excitation factor and/or coefficient have not been investigated. Taking the fact that they should also reside on the real axis into account, it is presumable that making full use of $A_{\rm in}$ on the real axis should give us a clue to these questions. Solving these problems will be helpful toward the era of future detectors such as the Laser Interferometer Space Antenna (LISA) [70], with which ringdown signals will be detected frequently with high signal-to-noise ratios, possibly accompanied by noticeable influences of surrounding environments.

ACKNOWLEDGMENTS

We thank Kouichi Hagino, Hidetoshi Omiya, and Norichika Sago for valuable discussions. This work was supported by Japan Society for the Promotion of Science (JSPS) Grants-in-Aid for Scientific Research (KAKENHI) Grants No. JP18H05236, No. JP20H00158, No. JP22K03617 (K. K.), No. JP18K13565, No. JP22K03639 (H. M.), and No. JP17H06357, No. JP17H06358, No. JP20K03928 (T. T.).

APPENDIX: SPECTRAL INSTABILITY FOR GENERIC TWO SEPARATED POTENTIALS

In Sec. III, we demonstrated that the spectral instability of quasinormal modes for double rectangular barriers is caused by a phase factor $e^{2i\omega b}$ by explicitly solving the scattering problem. In this appendix, we argue that this mechanism is a generic feature of two separated scattering potentials relying only on the asymptotic behavior of the solution (see also Ref. [52]).

First, we consider two potentials $V_A(r_*)$ and $V_B(r_*)$, both of which are localized around $r_*=0$ and admit plane wave solutions at $r_*\to\pm\infty$. Specifically, the "in" solution that becomes $e^{-i\omega r_*}$ at $r_*\to-\infty$ may be expressed at $r_*\to+\infty$ as

$$\tilde{\phi}_{\rm in}(r_*)=A_{\rm in}e^{-i\omega r_*}+A_{\rm out}e^{+i\omega r_*} \tag{A1}$$

and

$$\tilde{\phi}_{\rm in}(r_*)=B_{\rm in}e^{-i\omega r_*}+B_{\rm out}e^{+i\omega r_*}, \tag{A2}$$

for the potentials $V_A(r_*)$ and $V_B(r_*)$, respectively. This also implies that the solution that becomes $e^{+i\omega r_*}$ at $r_* \to -\infty$ is written as $B^*_{\rm in}e^{+i\omega r_*} + B^*_{\rm out}e^{-i\omega r_*}$ at $r_* \to +\infty$ for the potential $V_B(r_*)$.

Next, let us consider the potential given by $V(r_*) = V_A(r_*) + V_B(r_* - b)$, where b is chosen so large that Eq. (A1) is approximately valid at $0 \ll r_* \ll b$. By translating the radial coordinate, we readily found that the "in" solution for the potential $V(r_*)$ takes the asymptotic form of

$$\tilde{\phi}_{\rm in}(r_*) = (A_{\rm in}B_{\rm in} + A_{\rm out}B^*_{\rm out}e^{+2i\omega b})e^{-i\omega r_*} + (A_{\rm out}B^*_{\rm in} + A_{\rm in}B_{\rm out}e^{-2i\omega b})e^{+i\omega r_*}, \tag{A3}$$

at $r_* \to +\infty$. Finally, the Green's function with downgoing and outgoing boundary conditions is given in terms of the corresponding Wronskian,

$$W = 2i\omega(A_{\rm in}B_{\rm in} + A_{\rm out}B^*_{\rm out}e^{+2i\omega b}), \tag{A4}$$

which involves the phase factor $e^{+2i\omega b}$.

When the secondary potential $V_B(r_*)$ can be regarded as a perturbation to the primary potential $V_A(r_*)$, $|B_{\rm out}/B_{\rm in}| \ll |A_{\rm out}/A_{\rm in}| \leq 1$ holds. Thus, the second term in the Wronskian, Eq. (A4), is perturbative for the real frequency. However, the phase factor moves the poles of the Green's function on the complex frequency plane in an outspiraling manner as the value of b increases [18,23,52], causing the spectral instability.

[1] Emanuele Berti, Vitor Cardoso, and Andrei O. Starinets, Topical review: Quasinormal modes of black holes and black branes, Classical Quantum Gravity **26**, 163001 (2009).

[2] R. A. Konoplya and Alexander Zhidenko, Quasinormal modes of black holes: From astrophysics to string theory, Rev. Mod. Phys. **83**, 793 (2011).

[3] C. V. Vishveshwara, Scattering of gravitational radiation by a schwarzschild black-hole, Nature (London) **227**, 936 (1970).

[4] William H. Press, Long wave trains of gravitational waves from a vibrating black hole, Astrophys. J. Lett. **170**, L105 (1971).

[5] C. J. Goebel, Comments on the "vibrations" of a black hole, Astrophys. J. Lett. **172**, L95 (1972).

[6] Marc Davis, Remo Ruffini, William H. Press, and Richard H. Price, Gravitational Radiation from a Particle Falling Radially into a Schwarzschild Black Hole, Phys. Rev. Lett. **27**, 1466 (1971).

[7] Marc Davis, Remo Ruffini, and Jayme Tiomno, Pulses of gravitational radiation of a particle falling radially into a schwarzschild black hole, Phys. Rev. D **5**, 2932 (1972).

[8] C. T. Cunningham, R. H. Price, and V. Moncrief, Radiation from collapsing relativistic stars. I. Linearized odd-parity radiation, Astrophys. J. **224**, 643 (1978).

[9] C. T. Cunningham, R. H. Price, and V. Moncrief, Radiation from collapsing relativistic stars. II. Linearized even-parity radiation, Astrophys. J. **230**, 870 (1979).

[10] Fernando Echeverria, Gravitational-wave measurements of the mass and angular momentum of a black hole, Phys. Rev. D **40**, 3194 (1989).

[11] Lee S. Finn, Detection, measurement, and gravitational radiation, Phys. Rev. D **46**, 5236 (1992).

[12] Olaf Dreyer, Bernard Kelly, Badri Krishnan, Lee Samuel Finn, David Garrison, and Ramon Lopez-Aleman, Black-hole spectroscopy: Testing general relativity through gravitational-wave observations, Classical Quantum Gravity **21**, 787 (2004).

[13] Emanuele Berti, Vitor Cardoso, and Clifford M. Will, Gravitational-wave spectroscopy of massive black holes with the space interferometer LISA, Phys. Rev. D **73**, 064030 (2006).

[14] Jr. York and James W., Dynamical origin of black-hole radiance, Phys. Rev. D **28**, 2929 (1983).

[15] Shahar Hod, Bohr's Correspondence Principle and the Area Spectrum of Quantum Black Holes, Phys. Rev. Lett. **81**, 4293 (1998).

[16] Olaf Dreyer, Quasinormal Modes, the Area Spectrum, and Black Hole Entropy, Phys. Rev. Lett. **90**, 081301 (2003).

[17] José Luis Jaramillo, Rodrigo Panosso Macedo, and Lamis Al Sheikh, Pseudospectrum and Black Hole Quasinormal Mode Instability, Phys. Rev. X **11**, 031003 (2021).

[18] Mark Ho-Yeuk Cheung, Kyriakos Destounis, Rodrigo Panosso Macedo, Emanuele Berti, and Vitor Cardoso, Destabilizing the Fundamental Mode of Black Holes: The Elephant and the Flea, Phys. Rev. Lett. **128**, 111103 (2022).

[19] José Luis Jaramillo, Rodrigo Panosso Macedo, and Lamis Al Sheikh, Gravitational Wave Signatures of Black Hole Quasinormal Mode Instability, Phys. Rev. Lett. **128**, 211102 (2022).

[20] Hans-Peter Nollert, About the significance of quasinormal modes of black holes, Phys. Rev. D **53**, 4397 (1996).

[21] Ramin G. Daghigh, Michael D. Green, and Jodin C. Morey, Significance of black hole quasinormal modes: A closer look, Phys. Rev. D **101**, 104009 (2020).

[22] Wei-Liang Qian, Kai Lin, Cai-Ying Shao, Bin Wang, and Rui-Hong Yue, Asymptotical quasinormal mode spectrum for piecewise approximate effective potential, Phys. Rev. D **103**, 024019 (2021).

[23] Enrico Barausse, Vitor Cardoso, and Paolo Pani, Can environmental effects spoil precision gravitational-wave astrophysics?, Phys. Rev. D **89**, 104059 (2014).

[24] Emanuele Berti, Vitor Cardoso, Mark Ho-Yeuk Cheung, Francesco Di Filippo, Francisco Duque, Paul Martens, and Shinji Mukohyama, Stability of the fundamental

quasinormal mode in time-domain observations against small perturbations, Phys. Rev. D **106**, 084011 (2022).
[25] Matthew D. Duez and Yosef Zlochower, Numerical relativity of compact binaries in the 21st century, Rep. Prog. Phys. **82**, 016902 (2019).
[26] Luca Baiotti, Gravitational waves from neutron star mergers and their relation to the nuclear equation of state, Prog. Part. Nucl. Phys. **109**, 103714 (2019).
[27] The LIGO Scientific Collaboration, the Virgo Collaboration, and the KAGRA Collaboration, GWTC-3: Compact binary coalescences observed by LIGO and Virgo during the second part of the third observing run, arXiv:2111.03606.
[28] J. L. Jaramillo, Pseudospectrum and binary black hole merger transients, Classical Quantum Gravity **39**, 217002 (2022).
[29] Zachary Mark, Aaron Zimmerman, Song Ming Du, and Yanbei Chen, A recipe for echoes from exotic compact objects, Phys. Rev. D **96**, 084002 (2017).
[30] John R. Taylor, *Scattering Theory: The Quantum Theory of Nonrelativistic Collisions* (Dover Publications, New York, 2006).
[31] Tullio Regge and John A. Wheeler, Stability of a schwarzschild singularity, Phys. Rev. **108**, 1063 (1957).
[32] E. Gasperín and J. L. Jaramillo, Energy scales and black hole pseudospectra: The structural role of the scalar product, Classical Quantum Gravity **39**, 115010 (2022).
[33] S. Chandrasekhar, *The Mathematical Theory of Black Holes* (Springer, Dordrecht, 1983).
[34] Frank J. Zerilli, Effective Potential for Even-Parity Regge-Wheeler Gravitational Perturbation Equations, Phys. Rev. Lett. **24**, 737 (1970).
[35] S. Chandrasekhar and S. Detweiler, The quasi-normal modes of the schwarzschild black hole, Proc. R. Soc. A **344**, 441 (1975).
[36] Our normalization is chosen to match that of Ref. [18], in which quantities are normalized by $2M$. Our b/M corresponds to their $2a$.
[37] Richard H. Price, Nonspherical perturbations of relativistic gravitational collapse. I. Scalar and gravitational perturbations, Phys. Rev. D **5**, 2419 (1972).
[38] In this study, the "echo" signal broadly denotes any late-time component resulting from the existence of secondary potential peaks. The echo may be classified into high-frequency components associated with repeated reflections of unperturbed quasinormal modes and low-frequency components trapped in the cavity between two potential peaks.
[39] B. F. Schutz and C. M. Will, Black hole normal modes—A semianalytic approach, Astrophys. J. Lett. **291**, L33 (1985).
[40] Sai Iyer and Clifford M. Will, Black-hole normal modes: A WKB approach. I. Foundations and application of a higher-order WKB analysis of potential-barrier scattering, Phys. Rev. D **35**, 3621 (1987).
[41] Sai Iyer, Black-hole normal modes: A WKB approach. II. Schwarzschild black holes, Phys. Rev. D **35**, 3632 (1987).
[42] Yasuyuki Hatsuda, Quasinormal modes of black holes and Borel summation, Phys. Rev. D **101**, 024008 (2020).
[43] Kenichi Konishi and Giampiero Paffuti, *Quantum Mechanics: A New Introduction* (Oxford University Press, New York, 2009).
[44] Nils Andersson and Karl-Erik Thylwe, Complex angular momentum approach to black-hole scattering, Classical Quantum Gravity **11**, 2991 (1994).
[45] Nils Andersson, Complex angular momenta and the black-hole glory, Classical Quantum Gravity **11**, 3003 (1994).
[46] Yves Décanini, Antoine Folacci, and Bruce Jensen, complex angular momentum in black hole physics and quasinormal modes, Phys. Rev. D **67**, 124017 (2003).
[47] Emanuele Berti, Vitor Cardoso, and Paolo Pani, Breit-Wigner resonances and the quasinormal modes of anti-de Sitter black holes, Phys. Rev. D **79**, 101501 (2009).
[48] Yasuyuki Hatsuda and Masashi Kimura, Spectral problems for quasinormal modes of black holes, Universe **7**, 476 (2021).
[49] J. W. Guinn, C. M. Will, Y. Kojima, and B. F. Schutz, Letter to the editor: High-overtone normal modes of Schwarzschild black holes, Classical Quantum Gravity **7**, L47 (1990).
[50] Specifically in the standard terminology of one-dimensional quantum scatterings, in which R and T denote the reflection and transmission amplitudes for the potential, respectively, $A_{\rm in}$ and $A_{\rm out}$ may be expressed by $1/T$ and R/T, respectively.
[51] J. A. H. Futterman, F. A. Handler, and R. A. Matzner, *Scattering from Black Holes* (Cambridge University Press, Cambridge, England, 1988).
[52] P. T. Leung, Y. T. Liu, W. M. Suen, C. Y. Tam, and K. Young, Quasinormal Modes of Dirty Black Holes, Phys. Rev. Lett. **78**, 2894 (1997).
[53] Maximiliano Isi, Matthew Giesler, Will M. Farr, Mark A. Scheel, and Saul A. Teukolsky, Testing the No-Hair Theorem with GW150914, Phys. Rev. Lett. **123**, 111102 (2019).
[54] B. P. Abbott *et al.* (LIGO Scientific and Virgo Collaborations), Tests of general relativity with binary black holes from the second LIGO-Virgo gravitational-wave transient catalog, Phys. Rev. D **103**, 122002 (2021).
[55] Roberto Cotesta, Gregorio Carullo, Emanuele Berti, and Vitor Cardoso, Analysis of Ringdown Overtones in GW150914, Phys. Rev. Lett. **129**, 111102 (2022).
[56] Maximiliano Isi and Will M. Farr, Revisiting the ringdown of GW150914, arXiv:2202.02941.
[57] Strictly speaking, while the overtones are destabilized, the fundamental mode is not completely destabilized in our parameter set. We checked that our argument still holds for a parameter set where the fundamental mode is also destabilized.
[58] We note that the value of $V_1/V_0 \sim 10^{-3}$ adopted here is chosen to be so large that the effect of the second barrier becomes visible on the scale of this figure.
[59] E. W. Leaver, An analytic representation for the quasinormal modes of Kerr black holes, Proc. R. Soc. A **402**, 285 (1985).
[60] Eugene P. Wigner, Lower limit for the energy derivative of the scattering phase shift, Phys. Rev. **98**, 145 (1955).
[61] The transmission coefficient $1/|A_{\rm in}|^2$ is also called the graybody factor in the context of black-hole evaporation [62–64].
[62] S. W. Hawking, Black hole explosions?, Nature (London) **248**, 30 (1974).
[63] S. W. Hawking, Particle creation by black holes, Commun. Math. Phys. **43**, 199 (1975).

[64] Don N. Page, Particle emission rates from a black hole: Massless particles from an uncharged, nonrotating hole, Phys. Rev. D **13**, 198 (1976).
[65] Saul A. Teukolsky, Perturbations of a rotating black hole. I. Fundamental equations for gravitational, electromagnetic, and neutrino-field perturbations, Astrophys. J. **185**, 635 (1973).
[66] M. Sasaki and T. Nakamura, Gravitational radiation from a Kerr black hole. I—Formulation and a method for numerical analysis—, Prog. Theor. Phys. **67**, 1788 (1982).
[67] S. Chandrasekhar and S. Detweiler, On the equations governing the gravitational perturbations of the Kerr black hole, Proc. R. Soc. A **350**, 165 (1976).
[68] S. Detweiler, On resonant oscillations of a rapidly rotating black hole, Proc. R. Soc. A **352**, 381 (1977).
[69] Edward W. Leaver, Spectral decomposition of the perturbation response of the Schwarzschild geometry, Phys. Rev. D **34**, 384 (1986).
[70] J. Baker *et al.*, The laser interferometer space antenna: Unveiling the millihertz gravitational wave sky, arXiv:1907.06482.